GSA DATA REPOSITORY

DR1. DOLOMITE PETROGRAPHY AND O-C-SR ISOTOPE ANALYSES

Demonstrating that early-formed dolomites were affected by recrystallization commonly relies on conventional petrography and O-C-Sr isotope geochemistry arguments (e.g. Gregg et al., 1992; Montañez and Read, 1992; Kupecz and Land, 1994; Malone et al., 1994; Al-Aasm, 2000; Al-Aasm and Packard, 2000; Rott and Qing, 2013; Rahimi et al., 2016). With such scope, evaporative-sabkha and seepage-reflux dolomites from the Arab Fm. (Fig.1) have been sampled and investigated for thin section petrography (n= 79), oxygen and carbon stable isotopes (n= 37) and $^{87}Sr/^{86}Sr$ ratios (n=15), prior to perform Δ_{47}/U-Pb analyses.

Thin section (30 μm) petrography was accomplished at IFP Energies nouvelles. All thin sections were partially stained with a solution of 10% diluted HCl, Alizarin red-S and potassium ferricyanide (Dickson, 1966). A Nikon ECLIPSE LV100 POL polarized light microscope equipped with a mercury vapor lamp (100 W), allowed observations under plane-polarized (PPL), cross-polarized (CPL) and ultraviolet (UV) light. Cathodoluminescence (CL) microscopy was accomplished with a Nikon ECLIPSE ME600 equipped with a cold CL 8200 Mk5 CITL working under vacuum (<0.1 mBar) at 10 kV and 250 μA. Petrographic description was based on the dolomite texture classification from Sibley and Gregg (1987).

O and C stable isotope compositions ($\delta^{18}O_{dol}$, $\delta^{13}C_{dol}$) were measured at the University of Windsor (Canada). Carbonate powders were extracted from rock-slabs using a dental drill and a micro-mill (computer automated) device mounted on a binocular microscope. Samples were reacted with 100% phosphoric acid at 50 °C for four hours. The evolved CO_2 gas was analyzed for isotope ratios using a Delta-plus mass spectrometer. The phosphoric acid fractionation factors for dolomite at 50 °C were applied (Al-Aasm et al., 1990). The isotope compositions are reported in per mil (‰) relative to the Vienna Pee Dee Belemnite (V-PDB) standard. The reproducibility for $\delta^{18}O_{dol}$, $\delta^{13}C_{dol}$ was ±0.05‰ (1 std. dev.).

Sr isotope measurements were performed at Ruhr-Universität Bochum (Germany) by using 1 mg of dolomite powder dissolved in a 2.5 M HCl solution. The separation between the two components was done by the standard procedure of ionic exchange. The $^{87}Sr/^{86}Sr$ isotope ratios were determined using an automated Finnigan 261 mass spectrometer equipped with nine Faraday collectors. Correction for isotopic fractionation during the analyses was made by normalization to $^{86}Sr/^{88}Sr = 0.1194$. The mean standard error of mass spectrometer performance was ±0.00003 for standard NBS-987.

Among the whole samples investigated for petrography and O-C-Sr isotope geochemistry, 15 have been selected for Δ_{47}/U-Pb thermo-chronometry (Table DR4). The sample selection was based on: 1) the petrographic features in order to encompass different dolomite textures and crystal sizes observed; 2) the limited occurrence of non-dolomitic phases such as sulfates or calcite to avoid any mixing effect during analyses; 3) the variability of dolomite $\delta^{18}O_{dol}$ values, in order to cover a large spread in $\delta^{18}O_{dol}$; 4) the availability of sufficient material to realize thick sections (50-60 μm; for LA-ICPMS U-Pb dating) and to drill-sample mirror-like rock slabs (~15 mg for Δ_{47} thermometry).

Petrography was accomplished on all investigated dolomite samples belonging to supratidal facies (Dol1) and subtidal lagoon facies (Dol2). It revealed the occurrence of non-ferroan, fabric-preserving, dolomites with different textures (dolomicrite, planar-e, planar-s) except non-planar, and various crystal sizes (mostly <10 to 50 μm, and less commonly >50 μm). The dolomites are intimately associated with syn-depositional anhydrite nodules and beds or with early diagenetic anhydrite cements (Fig. DR1_A). All these features advocate for an early origin of the dolomites, in line with the evaporative-sabkha and seepage-reflux dolomitization models operating in a ramp system under an arid climate, as stated by previous authors investigating sedimentology, stratigraphy and diagenesis of the Arab Fm. (e.g. Grötsch et al., 2003; Cantrell, 2004; Swart et al., 2005; Al Suwaidi et al., 2005; Morad et al., 2012; Nader et

al., 2013; Lawrence et al., 2015; Marchionda et al. 2018). No later dolomite cements were recorded in the samples. Locally, other mineral phases (anhydrite and calcite) possibly post-dating the dolomites were observed; they fill fractures and intercrystalline pores in the dolomites and may locally replace some dolomite crystals (Fig. DR1_C).

No clear relationship was observed between dolomite petrography and Δ_{47}/U-Pb thermo-chronometry data (Fig. DR1_B). Indeed, when comparing samples with low temperatures (and old ages) and samples with high temperatures (and young ages) a clear increase in crystal size and/or in non-planar textures was not recorded. Furthermore, dolomite crystals display a uniform dull red CL and lack zonation/overgrowths and reaction borders, (Fig. DR1_B; Table DR4), that some authors have used as hints for recrystallization (e.g. Montañez and Read, 1992; Smith and Dorobek, 1993; Al-Aasm, 2000). Finally, UV-light microscopy revealed zoned crystals, with evidence of dolomite dissolution/reprecipitation, in only 5 dolomite samples, that encompass the whole range of the recorded $T\Delta_{47}$ temperatures (42-87 °C; Fig. DR1_B and Table DR4). These observations question the reliability of petrographic criteria to detect dolomite recrystallization like the observation of crystal coarsening, non-planar texture, and CL/UV-light responses (Gregg et al., 1992; Montañez and Read, 1992; Al-aasm, 2000; Al-Aasm and Packard, 2000; Smith and Dorobek, 1993). The application of such petrographic criteria to the investigated samples revealed not to be always consistent with the Δ_{47}/U-Pb data which disclosed recrystallization also in fine crystalline dolomites lacking non-planar textures and CL/UV-light heterogeneities.

However, it is worth mentioning that other hints for recrystallization may be revealed by methods not applied in the present study such as atomic force microscopy, allowing to investigate dolomite surface nanotopography (Kaczmarek and Sibley, 2014), and X-ray diffraction, allowing to evaluate stoichiometry and degree of cation ordering of dolomite

crystals (e.g. Montañez and Read, 1992; Kupecz and Land, 1994; Manche and Kaczmarek, 2021; Ryan et al., 2022).

Concerning geochemical proxies, the enrichment in ^{12}C and ^{87}Sr of dolomites is reported in literature as diagnostic of recrystallization (Gregg et al., 1992; Montañez and Read, 1992; Kupecz and Land, 1994; Malone et al., 1994; Rott and Qing, 2013). However, this is not observed in the studied samples which display $\delta^{13}C_{dol}$ and $^{87}Sr/^{86}Sr$ in agreement with: 1) carbonates precipitated in equilibrium with Late Jurassic seawater (Veizer et al., 1999); 2) limestones of the Arab Fm. from the same well cores here investigated (Morad et al., 2018, 2019). Furthermore, most of the measured $\delta^{13}C_{dol}$ and $^{87}Sr/^{86}Sr$ fall in a relatively narrow range irrespectively from the temperature/age recorded by Δ_{47}/U-Pb analyses (Fig. 2; Table DR1). This feature, together with the positive covariance between $\delta^{18}O_w$-$T\Delta_{47}$ (Fig. 2), points toward burial recrystallization occurring in a closed hydrologic system. Indeed, in such systems, the limited water/rock ratios would cause the newly formed carbonates (here the recrystallized dolomites) to have $\delta^{13}C_{dol}$ and $^{87}Sr/^{86}Sr$ values inherited from the original carbonates (Banner et al., 1988). This overall underlines how the geochemical proxies commonly used to detect dolomite recrystallization, may not be applied when the process occurs in closed hydrologic systems.

Table DR1. Name, well of belonging, depth, dolomite type, isotope compositions ($\delta^{18}O_{dol}$, $\delta^{13}C_{dol}$ and $^{87}Sr/^{86}Sr$) of 37 dolomite samples. The asterisks indicate the samples chosen to be further analyzed with Δ_{47}/U-Pb thermo-chronometry which results are reported in Table DR4.

Figure DR1_A. Core and petrographic images of the syn-depositional to early diagenetic anhydrite phases associated with the Arab Fm. dolomites from the studied field. **A.** Core image illustrating dolomudstone (grey), locally finely laminated, alternated with anhydrite

beds (white) forming enterolithic folds. **B.** Core image illustrating dolomudstone (grey) intimately associated with nodular to chicken-wire anhydrites (white). **C.** Petrographic image of a nodule composed by lath-shaped and felted crystals of anhydrite, surrounded by very fine crystalline dolomite (Dol1). Supratidal to intertidal facies. Plane-polarized light (PPL). **D.** Same image under cross-polarized light (CPL). **E.** Petrographic image of a pervasively dolomitized peloidal packstone. The fine crystalline dolomite (Dol2) is engulfed by a poikilotopic anhydrite cement. Subtidal facies. PPL. **F.** Same image under CPL.

Figure DR1_B. Petrographic features of some representative samples of Arab Fm. dolomites from the studied field under plane-polarized light (PPL), cathodoluminescence (CL) and ultraviolet-light (UV). In the inserts, are reported the Δ_{47} temperature (T), the $\delta^{18}O_w$ and the U-Pb age (t). **A.** Sample 20. PPL. **B.** Sample 18. PPL. **C.** Sample 16. PPL. **D.** Sample 12. PPL. **E.** Sample 22. PPL. **F.** Sample 4. PPL. **G.** Uniform dull red response under CL. Sample N20. **H.** Zoned crystals revealed under UV-light. Sample 22.

Figure DR1_C. Petrographic images of anhydrite and calcite phases possibly post-dating the Arab Fm. dolomites from the studied field under plane-polarized light (PPL) and cross-polarized light (CPL). **A.** Anhydrite phase filling intercrystalline pores and fractures in dolomites. PPL. **B.** Same image under CPL. **C.** Anhydrite phase filling a fracture in dolomites **D.** Same image under CPL **E.** Calcite phase (pink color revealed by staining) filling intercrystalline pores in dolomites. PPL. **F.** Anhydrite phase and calcite phase (pink color revealed by staining) filling intercrystalline pores in dolomites and replacing some dolomite crystals. PPL.

DR2. CLUMPED ISOTOPE (Δ_{47}) ANALYSES AND DATA PROCESSING

Simultaneous measurements of Δ_{47}, $\delta^{18}O$ and $\delta^{13}C$ compositions of carbonate samples were performed at Institut de Physique du Globe de Paris (IPGP) with a Thermo Scientific MAT253 gas-source mass spectrometer after digestion of carbonate powder in 104% phosphoric acid. About 5 mg of carbonate (dolomites) was reacted at 90°C in a common acid bath for 1 h. The methods used for carbonate digestion, CO_2 purification and isotope measurements follow the procedure detailed in Bonifacie et al. (2017). Each measurement consisted of 70 cycles of comparison between the CO_2 extracted from the sample against a working internal reference CO_2 gas [Oztech; with $\delta^{13}C = -3.72‰$ and $\delta^{18}O = -6.06‰$, *versus* VPDB (Vienna Pee Dee Belemnite), verified with the international carbonate reference material NBS19]. The signal integration time was 26 s (i.e. total integration time of 1820 s for each CO_2 sample) for a signal of 12V on m/z = 44. Each carbonate sample was analyzed two or three times to determine simultaneously its Δ_{47}, $\delta^{18}O$ and $\delta^{13}C$ compositions across distinct analytical sessions. The $\delta^{18}O$ and $\delta^{13}C$ carbonate compositions were acquired as part of each Δ_{47} analysis, and ^{17}O corrections were made using the parameters from Santrock et al. (1985). To account for the temperature dependence of oxygen isotope fractionation between CO_2 gas and carbonate, resulting from the reaction with phosphoric acid at 90°C, a fractionation factor of 1.093 for dolomite was used, following Rosenbaum & Sheppard (1986). The $\delta^{18}O$ and $\delta^{13}C$ of the dolomite samples are expressed in ‰ relative to the VPDB standard.

For constructing correction frames for processing raw Δ_{47} values, CO_2 gases driven to isotopologue equilibrium at both 1000°C and 25°C were used. The equilibrated CO_2 gas standards in this study have bulk isotopic compositions spanning the entire range of measured samples, were purified and analyzed in the same way as carbonate samples or carbonate standards and were typically run every four to five analyses. The raw Δ_{47} data were first

corrected for linearity effects using a fixed common equilibrated gas line slope fitted to the equilibrated CO_2 gases at both 1000°C and 25°C. Subsequently, the raw Δ_{47} values (expressed relative to the working gas) were transferred into the Carbon Dioxide Equilibrated Scale (CDES) using the CO_2 gases driven to isotopologue equilibrium at both 1000°C and 25°C with theoretically predicted Δ_{47} values of 0.0266‰ and 0.9252‰, respectively (after Wang et al., 2004). Finally, Δ_{47} data were projected into the 25°C acid digestion reference frame for easier comparison with previously published data (e.g. Swart et al. 2016). For this, an acid fractionation value of +0.092‰, determined by Henkes et al. (2013), was added.

To ensure accuracy of the entire data acquisition and reduction processes, and ultimately the accuracy of the Δ_{47} and $T\Delta_{47}$ data presented here, two carbonate reference materials were routinely analyzed (IPGP-Carrara marble and 102-GCAZ-01b). One of these two carbonate standards was analyzed typically every five analyses and distributed along the diagenetic cement samples and the equilibrated CO_2 gas standards in all runs, in order to check for analytical stability/accuracy of the whole procedure (including carbonate digestion, CO_2 purification, stability of the conditions for analyses of CO_2 inside the mass spectrometer and/or accuracy of the correction frames constructed with standards of equilibrated CO_2 gas – namely the accuracy of the equilibrated gas lines and empirical transfer function lines), as well as long-term reproducibility of the Δ_{47} measurements. Such analytical strategy respected the 1:1 ratio for standard: unknown sample recently recommended in Bernasconi et al. (2021) for accurate determination of Δ_{47} values. The Δ_{47} values obtained for these carbonate reference materials over the period of this study (November 2016 to December 2016) are: $\Delta_{47CDES90} = 0.426 \pm 0.023$‰ [1 SD (one standard deviation), n = 11] for IPGP-Carrara and $\Delta_{47CDES90} = 0.714 \pm 0.024$‰ (1 SD, n = 11) for 102-GC-AZ01b. These Δ_{47} values are indistinguishable from those obtained in previous studies (e.g. Dennis et al., 2011; Henkes et al., 2013) and on a longer timescale at IPGP (Bonifacie et al., 2017). Noticeably, when the

^{17}O parameters from Brand et al. (2010) are used to process isotopic data, as recommended by Daëron et al. (2016) and Schauer et al. (2016), such reprocessing only led to small differences in Δ_{47} values (i.e. less than ±0·010‰) of the standards and samples, within the analytical reproducibility on Δ_{47} measurements, and thus does not significantly change the reported temperatures (and conclusions) of this study. Finally, the corrected Δ_{47} values were then converted into temperatures ($T\Delta_{47}$) using the composite Δ_{47} -T calibration determined for all carbonate minerals for the 0 to 300°C temperature range [i.e. $\Delta_{47CDES25}$= 0.0422 * $10^6/T^2$ + 0.2182 Eq. 3 from Bonifacie et al. (2017)]. This equation was preferred to other recently published ones because generated with the exact same method (used for data acquisition and processing, including the same carbonate standards) and in the same laboratory as unknown samples analyzed here, limiting the error propagation arising from inter-laboratory inconsistencies (Bernasconi et al., 2021). The oxygen isotopic compositions of the water [$\delta^{18}O_w$, expressed in ‰ relative to the VSMOW (Vienna Standard Mean Ocean Water)] from which the dolomites precipitated (or were recrystallized) were calculated for each estimated $T\Delta_{47}$ using the $\delta^{18}O_{dol}$ values measured, as well as the oxygen isotope fractionation between the dolomite and water from Horita (2014).

DR3. U-PB GEOCHRONOLOGY BY LA-ICPMS: DATA ACQUISITION AND PROCESSING

Uranium and Pb isotopic ratios were measured in situ on thin sections (30-60µm thick) by LA-ICP-MS at Frankfurt Isotope and Element Research Center (FIERCE) of the Goethe University of Frankfurt using a method similar to that described in Gerdes and Zeh (2006). The measurements were acquired using a Thermo-Scientific Element XR ICP-MS, coupled to a RESOlution (Resonetics) 193 nm ArF Excimer laser (CompexPro 102, Coherent) equipped with a S-155 two-volume ablation cell (Laurin Technic, Australia). Signal strength at the ICP-MS was tuned for maximum sensitivity while keeping oxide formation below 0.3% (UO/U) and element fraction low (e.g., Th/U = 1). The data were acquired in fully-automated mode overnight in three different analytical sessions during which a spot size of 213µm was used. All other parameters and the tuning conditions of the mass spectrometer were kept constant between the sessions. Samples were ablated with a fluence of < 2 J cm^2 at 12 Hz in a helium atmosphere (0.3 l/min) and mixed in the ablation funnel with 0.9 l/min argon and 0.06 l/min nitrogen. For a 213 µm spot this yielded for SRM-NIST614 a depth penetration of about 0.6 µm s-1 and an average sensitivity of 420000 cps/µg g-1 for ^{238}U. The detection limits (4 x background signal) for ^{206}Pb and 238U were ~ 0.1 and 0.03 ppb, respectively. However, at a U signal of less 1000 cps (~ 2 ppb) the data were generally discarded due to enhance scatter on the isotope ratios. Each analysis consisted of 20 s of background acquisition followed by 20 s of sample ablation and 25 s of washouts. During 42 s data acquisition, the signal of ^{206}Pb, ^{207}Pb, ^{232}Th and ^{238}U were detected by peak jumping in pulse counting mode with a total integration time of 0.1 s, resulting in 420 mass scans. Prior to analysis each spot was pre-ablated for 5 s to remove surface contamination. Raw data were corrected offline using a macro-based in-house MS Excel© spreadsheet program. Following background correction, outliers (± 2s) were rejected based on the time-resolved $^{207}Pb/^{206}Pb$

and $^{206}Pb/^{238}U$ ratios together with the Pb and U signal. Due to fast washout, the low volume cell allows to detect inhomogeneity of the ablated material during depth profiling at a level of <0.8µm (<1s). Soda-lime glass SRM-NIST614 (RM-0) was used as a reference glass together with 3 carbonate standards to bracket sample analysis. The $^{207}Pb/^{206}Pb$ ratio was corrected for mass bias (~0.3%) and the $^{206}Pb/^{238}U$ ratio for inter-element fractionation (~9%), including drift over the sequence time, using the SRM-NIST 614.

Correction for sample matrix effects on the $^{238}U/^{206}Pb$ ratio of 3% was made by using a natural calcite spar named WC-1 (Roberts et al. 2017). This natural carbonate is commonly used as reference material for normalization of the $^{238}U/^{206}Pb$ ratio (Li et al., 2014; Coogan et al., 2016; Methner et al., 2016; Roberts and Walker, 2016, Godeau et al., 2018).

The $^{206}Pb/^{238}U$ downhole fractionation during 20s depth profiling was estimated to be 1-2% based on the common Pb corrected WC-1 analyses, which has been applied as an external correction to all carbonate analyses. Reported uncertainties (2σ) of the $^{206}Pb/^{238}U$ and $^{207}Pb/^{206}Pb$ ratios were propagated by quadratic addition of the excess of scatter (NIST-SRM 614), the excess of variance (WC-1), uncertainties derived from counting statistics and background and the precision of each analysis (2 SE; standard error).

Multi-spot analyses ($13<n<92$) were performed on single carbonate domains previously characterized by cathodoluminescence imaging. Samples were screened before analysis to aim for the highest variability on the $^{238}U/^{206}Pb$ versus $^{207}Pb/^{206}Pb$ by targeting domains with very low U containing mostly initial common Pb and ones with the highest possible radiogenic Pb component as result of the U decay.

Analyses are plotted along in the Tera-Wasserburg Concordia diagram, and the age is defined by the slope of the regression line and the lower intercept with the Concordia. The precision on that age directly depend on the variability of the $^{238}U/^{206}Pb$, the uncertainty on the isotope ratios and the overall statistical fit of the regression line (c.f. MSWD; Brooks et al. 1972).

Repeated analyses (n = 24) of a stromatolitic limestone from the Cambrian-Precambrian boundary in South-Namibia (Feldschuhhorn below Spitskopf formation, Schwarzrand subgroup ; Salor et al. 1996) yielded lower intercept ages of 541.9 ± 5.0 Ma (MSWD = 1.5). This is within uncertainty identical to the U/Pb zircon age of 543 ± 1 Ma from an ash layer of the Spitskopf formation (Bowring et al. 1993). Multiple spots (n = 26) of ASH15 yielded a lower intercept age of 3.001 ± 0.118 (MSWD = 0.56) and an upper intercept of 0.864 for the initial $^{207}Pb/^{206}Pb$. This is identical within uncertainty of the U-Pb age reported by Nuriel et al. (2021) using the conventional ID-TIMS method. Spot analyses (n = 20) of a Zechstein dolomite (Gypsum pit, Tettenborn, Germany; in-house reference material) yielded a lower intercept age of 256.1 ± 5.7 Ma identical to previously obtained ages at FIERCE (e.g. Burisch et al. 2018) and consistent with an early diagenetic origin.

The data of the carbonate (calcite and dolomite) reference material imply an accuracy and repeatability of the method of 1-2% providing the material has sufficient spread in the U/Pb. This is also supported by results of Godeau et al. (2018) where samples analyzed with the same device and by using the same method as described here agreed within uncertainy (+/- 1%) with ID solution mode analysis. The analytical data are summarized in Table DR4 and presented in detail in Table DR5. This latter contains the complete analytical data set of the 3 analytical sessions including that of the reference material and the Metadata table. Data were plotted in the Tera-Wasserburg diagram (Extended Data) and ages calculated as lower intercepts using Isoplot 3.71 (www.Isoplot.com). All uncertainties are reported at the 2σ level.

DR4. FURTHER DISCUSSION ON Δ_{47}/U-PB THERMO-CHRONOMETRY

Additional data on the 15 dolomite samples investigated with Δ_{47}/U-Pb thermo-chronometry are reported in Figure DR4_A and Table DR4.

Constraints on the thermal history of the studied samples (presently at 2833-3366 m depth) are needed to interpret the Δ_{47} dataset here presented. A burial curve for the Arab Fm. from both crest and flank of the studied anticline field is available from Al Darmaki et al. (2014) who applied back-stripping analysis. Accordingly, the investigated reservoir unit from the anticline crest reached peak burial conditions (~3 km) in the Miocene. A present-day geothermal gradient of 38 °C/km was calculated from bottom hole temperatures of crest and flank wells (Morad et al., 2019) and here extrapolated into the past. This geothermal gradient, together with a surface temperature of 20 °C and the available burial curve allowed reconstructing the thermal history illustrated in Figure 3. Accordingly, the thermal maximum reached in the Miocene by the studied rocks was estimated to be ~140 °C. Similarly, by considering geothermal gradients of 35 °C/km and 45 °C/Km thermal maximum respectively of ~135 °C and ~160 °C were estimated (Fig. 3).

The Δ_{47} response of dolomites that precipitated under ambient temperature conditions and experienced burial was evaluated by considering these two end-member thermal histories. Indeed, it is known that carbonates heated above their original precipitation temperatures over geological times may experience solid-state reordering of C-O bonds, partially resetting the original C-O bond ordering state and resulting in apparent TΔ_{47} which exceed the real precipitation temperatures (Passey and Henkes, 2012; Stolper and Eiler, 2015; Lawson et al., 2017; Lloyd et al., 2018; Hemingway and Henkes, 2021). Two carbonate Δ_{47} reordering models were here considered to account for solid-state reordering of the Arab Fm. dolomites: 1) the exchange-diffusion model from Stolper and Eiler (2015) by employing the

ClumpyCool package for Python of Lloyd et al. (2018); 2) the disordered kinetic model from Hemingway and Henkes (2021).

Both reordering models were run such that at time t_0 the Δ_{47} values of dolomite were in equilibrium with surface temperatures (20°C) and by considering the thermal histories reconstructed via geothermal gradients comprised between 35 °C/km and 45 °C/km, with the present-day gradient being 38 °C/km. Results of dolomite Δ_{47} reordering models are illustrated in Figure DR4_B. The first model indicates that dolomite Δ_{47} compositions start to undergo reordering only when the 45 °C/km geothermal gradient is considered, whereas the second model predicts no reordering. Being the 45 °C/km gradient unlikely for the intracratonic basin investigated (Bostick, et al. 1978, Moeck, 2014, Selley and Sonnenberg, 2023), it can be concluded that the $T\Delta_{47}$ measured for the Arab Fm. dolomites confidently reflect the temperatures of dolomite original precipitation or of subsequent recrystallization.

Figure DR4_A. $^{238}U/^{206}Pb$ versus $^{207}Pb/^{206}Pb$ Tera-Wasserburg Concordia diagrams and corresponding lower intercept ages of the 11 dolomite samples dated. Data point error ellipses indicate 2σ internal uncertainty of the isotope ratios on "n" analyses. Red lines represent the envelopes of the regression lines (isochrons). MSWD stands for Mean Standard Weighted Deviates.

Table DR4. Details on the dolomite samples analyzed for Δ_{47}/U-Pb thermo-chronometry: sample name, well of provenance, dolomite type, CL and UV-light response, are illustrated together with data resulting from Δ_{47} thermometry and LA-ICPMS U-Pb geochronology.

Figure DR4_B.

Modelling of the Δ_{47} reordering behavior of dolomite precipitated at 20 °C. The black lines define the thermal history suffered by the studied samples when considering different geothermal gradients: the present-day 38 °C/km (dotted line) and 45 °C/km (solid line). The colored lines indicate the evolution of $T\Delta_{47}$ over time when considering different reordering models. **To the left**: Predictions from the Stolper and Eiler (2015) model using the code of Lloyd et al. (2018) are illustrated; dolomite Δ_{47} starts to suffer reordering only when the 45 °C/km geothermal gradient is considered (solid red line). **To the right**: Predictions from the Hemingway and Henkes (2021) model indicate no significant reordering of dolomite Δ_{47} even when considering the 45 °C/km geothermal gradient (solid orange line).**DR5. U-PB**

GEOCHRONOLOGY RAW DATA

Table DR5. Raw data of U-Pb LA-ICPMS geochronology can be found online. The dataset is corrected offline using a macro-based in-house MS Excel© spreadsheet.

REFERENCES CITED IN THE DATA REPOSITORY

Al-Aasm, I.S., Taylor, B.E., South, B., 1990. Stable isotope analysis of multiple carbonate samples using selective acid extraction. Chemical Geology: Isotope Geoscience Section, 80(2), 119–125. DOI:10.1016/0168-9622(90)90020-D

Al-Aasm, I.S., 2000. Chemical and isotopic constraints for recrystallization of sedimentary dolomites from the Western Canada Sedimentary Basin. Aquatic Geochemistry, 6: 227-248. DOI:10.1023/A:1009611224589

Al-Aasm, I.S., Packard, J.J., 2000. Stabilization of early-formed dolomite: a tale of divergence from two Mississippian dolomites. Sedimentary Geology, 131, 97-108. DOI:10.1016/S0037-0738(99)00132-3

Al-Darmaki, F., Mattner, J., Bouzida, Y., Cavailhes, T., Burreson, M., Lawrence, D. A., Lucas, N., 2014. Identification, upscaling and modeling strategy for multi-scale fracture networks in variable lithology reservoirs: case study from a giant onshore UAE gas field. In: EAGE Borehole Geology Workshop,12-15 October 2014, Dubai, UAE. DOI:10.3997/2214-4609.20142332

Al Suwaidi, A.S., El Hami, M., Hagiwara, H., Aziz, S.K., Al Habshi, A.R., 2011. Carbonates and evaporites of the Upper Jurassic Arab Formation, Abu Dhabi: a petroleum exploration challenge. In: Kendall, C.G.S.C., Alsharhan, A.S. (eds) Quaternary carbonate and evaporite sedimentary facies and their ancient analogues: a tribute to Douglas James Shearman, 43. International Association of Sedimentologists, 421–430. DOI: 10.1002/9781444392326.ch19

Banner, J. L., Hanson, G.N., Meyers, W.J., 1988. Water-rock interaction history of regionally extensive dolomites of the Burlington-Keokuk Formation (Mississippian): isotopic evidence. In: Shukla, V., Baker, P. (eds), Sedimentology and geochemistry of dolostones. SEPM Special Publication, 43, 97–113. DOI:10.2110/pec.88.43.0097

Bernasconi, S.M., Daëron, M., Bergmann, K.D., Bonifacie, M., Meckler, A.N., Affek, H.P., Anderson, N., Bajnai, D., Barkan, E., Beverly, E., Blamart, D., Burgener, L., Calmels, D., Chaduteau, C., Clog, M., Davidheiser-Kroll, B., Davies, A., Dux, F., Eiler, J., Elliott, B., Fetrow, A.C., Fiebig, J., Goldberg, S., Hermoso, M., Huntington, K.W., Hyland, E., Ingalls, M., Jaggi, M., John, C.M., Jost, A.B., Katz, S., Kelson, J., Kluge, T., Kocken, I.J., Laskar, A., Leutert, T.J., Liang, D., Lucarelli, J., Mackey, T.J., Mangenot, X., Meinicke, N., Modestou, S.E., Müller, I.A., Murray, S., Neary, A., Packard, N., Passey, B.H., Pelletier, E., Petersen, S., Piasecki, A., Schauer, A., Snell, K.E., Swart, P.K., Tripati, A., Upadhyay, D., Vennemann, T., Winkelstern, I., Yarian, D., Yoshida, N., Zhang, N., Ziegler, M., 2021. InterCarb: A Community Effort to Improve Interlaboratory Standardization of the Carbonate Clumped Isotope Thermometer Using Carbonate Standards. Geochemistry, Geophysics, Geosystems, 22 (5), e2020GC009588. DOI:10.1029/2020GC009588

Bonifacie, M., Calmels, D., Eiler, J.M., Horita, J., Chaduteau, C., Vasconcelos, C., Agrinier, P., Katz, A., Passey, B.H., Ferry, J.M., Bourand, J.J., 2017. Experimental calibration of the dolomite clumped isotope thermometer from 25 to 350°C, and implications for the temperature estimates for all (Ca, Mg, Fe) CO3 carbonates digested at high temperature. Geochimica et Cosmochimica Acta, 200, 255-279. DOI:10.1016/j.gca.2016.11.028

Bostick, N.H., Cashman, S.M., McCulloh, T.H., Waddell, C.T., 1978. Gradients of vitrinite reflectance and present temperature in the Los Angeles and Ventura Basins, California. In: Oltz, D.F. (ed.): A Symposium in Geochemistry: Low Temperature Metamorphism of Kerogen and Clay Minerals. Los Angeles, Pacific Section, Society of Economic Paleontologists and Mineralogists, 65–96.

Bowring, S. A., Grotzinger, J.P., Isachsen, C.E., Knoll, A.H., Pelechaty, S.M. and Kolosov, P., 1993. Calibrating rates of Early Cambrian evolution. Science, 261, 1293-1298. DOI:10.1126/science.11539488

Brand, W.A., Assonov, S.S. and Coplen, T.B., 2010. Correction for the ^{17}O interference in $\delta(^{13}C)$ measurements when analyzing CO_2 with stable isotope mass spectrometry. Pure Appl. Chem., 82, 1719–1733. DOI: 10.1351/PAC-REP-09-01-05

Brooks, C., I. Wendt, and S. R. Hart, 1972. Realistic use of 2-error regression treatments as applied to rubidium-strontium data. Rev. Geophys., 10, 551–577. DOI:10.1029/RG010i002p00551

Burisch, M., Walter, B.F., Gerdes, A., Lanz, M., Markl, G., 2018. Late-stage anhydrite-gypsum-siderite-dolomite-calcite assemblages record the transition from a deep to a shallow hydrothermal system in the Schwarzwald mining district, SW Germany. Geochimica et Cosmochimica Acta, 223, 259-278, DOI :10.1016/j.gca.2017.12.002.

Cantrell, D. Swart, P., Hagerty, R., 2004. Genesis and characterization of dolomite Arab-D reservoir, Ghawar Field, Saudi Arabia: Geo-Arabia, v. 9, p. 11–36.

Coogan, L.A., Parrish, R.R., and Roberts, N.M.W., 2016. Early hydrothermal carbon uptake bythe upper oceanic crust: Insight from in situ U-Pb dating. Geology, 44, 147–150. DOI:10.1130/G37212.1

Daëron, M., Blamart, D., Peral, M., Affek, H., 2016. Absolute isotopic abundance ratios and the accuracy of Δ_{47} measurements. Chemical Geology, 442, 83. DOI:10.1016/j.chemgeo.2016.08.014

Dennis, K.J., Affek, H.P., Passey, B.H., Schrag, D.P., Eiler, J.M., 2011. Defining an absolute reference frame for 'clumped' isotope studies of CO_2. Geochimica et Cosmochimica Acta, 75, 7117–7131. DOI:10.1016/j.gca.2011.09.025

396 Dickson, J.A.D., 1966. Carbonate identification and genesis as revealed by staining. J.
397 Sediment. Res., 36 (2), 491–505. DOI :10.1306 /74D714F6-2B21-11D7-
398 8648000102C1865D.
399 Gerdes, A. and Zeh, A., 2006. Combined U-Pb and Hf isotope LA-(MC-) ICP-MS analyses
400 of detrital zircons: comparison with SHRIMP and new constraints for the provenance
401 and age of an Armorican metasediment in Central Germany. Earth and Planetary
402 Science Letters, 249, 47–61.
403 Godeau, N., Deschamps, P., Guihou, A., Leonide, P., Tendil, A., Gerdes, A., Hamelin, B.,
404 and
405 Girard, J.P., 2018, U-Pb dating of calcite cement and diagenetic history in microporous
406 carbonate reservoirs: Case of the Urgonian Limestone, France. Geology, 46, 247–250.
407 DOI:10.1130/G39905.1
408 Gregg, J.M., Howard, S.A., Mazzullo, S.J., 1992. Early diagenetic recrystallization of
409 Holocene (<3000 years old) peritidal dolomites, Ambergris Cay, Belize.
410 Sedimentology, 39, 143-159. DOI:10.1111/j.1365-3091.1992.tb01027.x
411 Grötsch, J., Suwaina, O., Ajlani, G., Taher, A., El-Khassawneh, R., Lokier, S., Coy, G., Van
412 der Weerd, E., Masalmeh, S., Van Dorp, J., 2003. The Arab Formation in central Abu
413 Dhabi: 3-D reservoir architecture and static and dynamic modeling. GeoArabia 8 (no.
414 1), 47–86.Hemingway, J.D, Henkes, G.A., 2021. A disordered kinetic model for
415 clumped isotope bond reordering in carbonates. Earth and Planetary Science Letters,
416 566, 116962. DOI: 10.1016/j.epsl.2021.116962
417 Henkes, G.A., Passey, B.H., Wanamaker, A.D., Grossman, E.L., Ambrose, W.G., Carroll,
418 M.L., 2013. Carbonate clumped isotope compositions of modern marine mollusk and
419 brachiopod shells. Geochim. Cosmochim. Acta, 106, 307–325.
420 DOI:10.1016/j.gca.2012.12.020

421 Horita, J., 2014. Oxygen and carbon isotope fractionation in the system dolomite–water–CO_2
422 to elevated temperatures. Geochimica et Cosmochimica Acta, 129, 111– 24.
423 DOI:10.1016/j.gca.2013.12.027
424 Kaczmarek, S.E., Sibley, D.F., 2014. Direct physical evidence of dolomite recrystallization.
425 Sedimentology, 61, 1862-1882. DOI:10.1111/sed.12119
426 Kupecz, J.A., Land, L.S., 1994. Progressive recrystallization and stabilization of early-stage
427 dolomite: Lower Ordovician Ellenburger Group, West Texas. In: Purser, B., Tucker,
428 M., Zenger, D. (eds), Dolomites: a volume in honour of Dolomieu. IAS Special
429 Publication, 255-279. DOI:10.1002/9781444304077.ch15
430 Lawrence, D.A., Hollis, C., Green, D., Deville de Perière, M., Al Darmaki, F., Bouzida, Y.,
431 2015. Paleogeographic reconstruction of a tide-dominated oolite shoal complex in
432 the lower Arab Formation, onshore UAE. In: Abu Dhabi International Petroleum
433 Exhibition and Conference, pp. 1–21 9-12 November, Abu Dhabi, UAE. SPE paper
434 172769-MS.
435 Lawson, M., Shenton, B. J., Stolper, D. A., Eiler, J. M., Rasbury, E. T., Becker, T. P., Pottorf,
436 R., Grey, G. G., Yurewicz, D., & Gournay, J. (2018). Deciphering the diagenetic
437 history of the El Abra Formation of eastern Mexico using reordered clumped isotope
438 temperatures and U-Pb dating. GSA Bulletin, 130 (3-4), 617-629.
439 DOI:10.1130/B31656.1
440 Li, Q., Parrish, R.R., Horstwood, M.S., and McArthur, J.M., 2014. U–Pb dating of cements in
441 Mesozoic ammonites: Chemical Geology, 376, 76–83.
442 DOI:10.1016/j.chemgeo.2014.03.020
443 Lloyd, M.K., Ryb, U., Eiler, J.M., 2018. Experimental calibration of clumped isotope
444 reordering in dolomite. Geochimica et Cosmochimica Acta, 242, 1-20.
445 DOI:10.1016/j.gca.2018.08.036

446 Malone, M.J., Baker, P.A., Burns, S.J., 1994. Recrystallization of dolomite: evidence from
447 the Monterey Formation (Miocene) California. Sedimentology, 41, 1223-1239.
448 DOI:10.1111/j.1365-3091.1994.tb01450.x
449 Manche, C.J. and Kaczmarek, S.E., 2021. A global study of dolomite stoichiometry and
450 cation ordering through the phanerozoic. J. Sediment. Res., 91, 520–546.
451 Marchionda, E., Deschamps, R., Cobianchi, M., Nader, F.H., Di Giulio, A., Morad, D.J., Al
452 Darmaki, F., Ceriani, A., 2018. Field-scale depositional evolution of the Upper Jurassic Arab
453 Formation (onshore Abu Dhabi, UAE). Mar. Petrol. Geol. 89, 350–369. DOI:
454 10.1016/j.marpetgeo.2017.10.006Methner, K., Mulch, A., Fiebig, J., Wacker, U., Gerdes, A.,
455 Graham, S.A., and Chamberlain,
456 C.P., 2016. Rapid Middle Eocene temperature change in western North America. Earth
457 and Planetary Science Letters, 450, 132–139. DOI:10.1111/sed.12427
458 Moeck, I.S., 2014. Catalog of geothermal play types based on geologic controls. Renewable
459 and Sustainable Energy Reviews, 37, 867–882. DOI:10.1016/j.rser.2014.05.032
460 Morad, S., Al-Aasm, I.S., Nader, F.H., Ceriani, A., Gasparrini, M., Mansurbeg, H., 2012.
461 Impact of diagenesis on the spatial and temporal distribution of reservoir quality in the
462 Jurassic Arab D and C members, offshore Abu Dhabi oilfield, United Arab Emirates.
463 GeoArabia, 17(3), 17-56.
464 Montañez, I.P., Read, J.F., 1992. Fluid-rock interaction history during stabilization of early
465 dolomites, Upper Knox Group (Lower Ordovician), US Appalachians. Journal of
466 Sedimentary Petrology, 62, 753-778. DOI:10.1306/D42679D3-2B26-11D7-
467 8648000102C1865DMorad, D., Nader, F.H., Gasparrini, M., Morad, S., Rossi, C.,
468 Marchionda, E., Al Darmaki, F., Martines, M., Hellevang, H., 2018. Comparison of the
469 diagenetic and reservoir quality evolution between the anticline crest and flank of an

Upper Jurassic carbonate gas reservoir, Abu Dhabi, United Arab Emirates. Sedimentary Geology 367, 96–113. DOI:10.1016/j.sedgeo.2018.02.008

Morad, D., Nader, F.H., Morad, S., Rossi, C., Gasparrini, M., Al Darmaki, F., Hellevang, H., 2019. Limited thermochemical sulfate reduction (TSR) in hot sour gas carbonate - anhydritic reservoirs of the Upper Jurassic Arab Formation, United Arab Emirates. Marine and Petroleum Geology, 106, 30-41. DOI:10.1016/j.marpetgeo.2019.04.023

Nader, F.H., De Boever, E., Gasparrini, M., Liberati, M., Dumont, C., Ceriani, M., Morad, S., Lerat, O., Doligez, B., 2013. Quantification of diagenesis impacts on reservoir properties of the Jurassic Arab D and C members (offshore, U.A.E). Geofluids, 13(2): 204-220. DOI: 10.1111/gfl.12022Nuriel, P., Wotzlaw, J.F., Ovtcharova, M., Vaks, A., Stremtan, C., Šala, M., Roberts, N.M.W., Kylander-Clark, A.R.C., 2021. The use of ASH-15 flowstone as a matrix-matched reference material for laser-ablation U − Pb geochronology of calcite, Geochronology, 3, 35-47.Passey, B.H., Henkes, G.A., 2012. Carbonate clumped isotope bond reordering and geospeedometry. Earth and Planetary Science Letters, 351-352, 223-236. DOI:10.1016/j.epsl.2012.07.021

Rahimi, A., Adabi, M.H., Aghanabati, A., Majidifard, M.R., Jamali, A.M., 2016. Dolomitization mechanism based on petrography and geochemistry in the Shotori Formation (Middle Triassic), Central Iran. Open Journal of Geology, 6, 1149-1168. DOI:10.4236/ojg.2016.69085

Ryan, B.H., Kaczmarek, S.E., Rivers, J.M., Manche, C.J., 2022. Extensive recrystallization of Cenozoic dolomite during shallow burial: A case study from the Palaeocene–Eocene Umm er Radhuma formation and a global meta-analysis. Sedimentology, 69(5), 2053-2079. DOI: 10.1111/sed.12982Roberts, N.M.W., and Walker, R.J., 2016. U-Pb geochronology of calcite-mineralized faults:

Absolute timing of rift-related fault events on the northeast Atlantic margin. Geology,

44, 531–534. DOI:10.1130/G37868.1

Roberts, N. M. W., Rasbury, E. T., Parrish, R. R., Smith, C. J., Horstwood, M. S. A., Condon, D. J., 2017. A calcite reference material for LA-ICP-MS U-Pb geochronology, Geochem. Geophy., Geosy., 18, 2807-2814

Rosenbaum, J., Sheppard, S. M. F., 1986. An isotopic study of siderites, dolomites and ankerites at high temperatures. Geochimica et Cosmochimica Acta, 50(6), 1147-1150. DOI: 10.1016/0016-7037(86)90396-0

Rott, C.M., Qing, H., 2013. Early dolomitization and recrystallization in shallow marine carbonates, Mississippian Alida beds, Williston basin (Canada): evidence from petrography and isotope geochemistry. Journal of Sedimentary Research, 83, 928-941. DOI:10.2110/jsr.2013.73

Selley, R.C., Sonnenberg, S.A., 2023. Sedimentary basins and petroleum systems. In: R.C., Selley, S.A, Sonnenberg (eds), Elements of Petroleum Geology. Forth Edition. Academic Press, 419-472.

Santrock, J., Studley, S.A., Hayes, J.M., 1985. Isotopic analyses based on the mass spectrum of carbon dioxide. Analytical Chemistry, 57, 1444–1448. DOI:10.1021/ac00284a060

Schauer, A.J., Julia Kelson, J., Saenger, C., Huntington, K.W., 2016. Choice of ^{17}O correction affects clumped isotope (Δ_{47}) values of CO_2 measured with mass spectrometry. Rapid Communications in Mass Spectrometry, 30, 2607–2616. DOI:10.1002/rcm.7743

Sibley, D.F., Gregg, J.M., 1987. Classification of dolomite rock textures. Journal of Sedimentary Petrology, 57, 967-975. DOI:10.1306/212F8CBA-2B24-11D7-8648000102C1865D

Smith, T.M., Dorobek, S.L., 1993. Alteration of early-formed dolomite during shallow to deep burial: Mississippian Mission Canyon Formation, central to southwestern

Montana. Geological Society of America Bulletin, 105, 1389–1399. DOI:10.1130/0016-7606(1993)105<1389:AOEFDD>2.3.CO;2

Stolper, D.A., Eiler, J.M., 2015. The kinetics of solid-state isotope-exchange reactions for clumped isotopes: A study of inorganic calcites and apatites from natural and experimental samples. American Journal of Science, 315 (5), 363-411. DOI:10.2475/05.2015.01

Swart, P.K., Cantrell, D.L., Westphal, H., Handford, C.R., Kendall, C.G., 2005. Origin of dolomite in the Arab-D reservoir from the Ghawar field, Saudi Arabia: evidence from petrographic and geochemical constraints. Journal of Sedimentary Research, 75, 476-491. DOI:10.2110/jsr.2005.037

Swart, P.K., Cantrell, D.L., Arienzo, M.M., Murray, S.T., 2016. Evidence for high temperature and 18O-enriched fluids in the Arab-D of the Ghawar Field, Saudi Arabia. Sedimentology, 63, 1739-1752. DOI:10.1111/sed.12286

Veizer, J., Ala, D., Azmy, K., Bruckschen, P., Buhl, D., Bruhn, F., Garden, G.A.F., Diener, A., Ebneth, S., Godderis, Y., Japer, T., Korte, C., Pawellek, F., Podlaha., O.G. Strauss, H., 1999. $^{87}Sr/^{86}Sr$, $\delta^{13}C$ and $\delta^{18}O$ evolution of Phanerozoic seawater. Chemical Geology, 161, 59–88. DOI:10.1016/S0009-2541(99)00081-9

Wang, Z., Schauble, E.A. and Eiler, J.M. (2004) Equilibrium thermodynamics of multiply substituted isotopologues of molecular gases. Geochim. Cosmochim. Acta, 68(23), 4779-4797.

Sample ID[1]	Well	Depth (m)	Dolomite type	$\delta^{18}O_{dol}$ (‰, VPDB)[2]	$\delta^{13}C_{dol}$ (‰, VPDB)[2]	$^{87}Sr/^{86}Sr$
1	C	3303.1	Dol1	-1.72	-0.12	-
2	C	3304.2	Dol1	-1.88	-0.32	-
3	C	3308.8	Dol2	-3.24	-1.02	0.707182
4*	C	3309.7	Dol2	-2.51	0.14	0.707033
5	C	3310.4	Dol1	-2.60	0.35	0.707142
6	C	3310.7	Dol2	-2.19	0.54	0.707000
7	C	3312.1	Dol1	-2.96	-1.31	-
8	C	3314.3	Dol1	-2.56	-0.12	-
9	C	3316.4	Dol1	-2.64	-0.68	-
10	C	3317.3	Dol1	-2.38	-1.00	-
11	C	3318.0	Dol2	-3.83	-1.12	-
12*	C	3318.9	Dol2	-2.39	-0.40	0.707056
13	C	3319.7	Dol2	-2.95	-0.44	0.707020
14	C	3324.4	Dol2	-5.71	0.56	0.706955
15*	C	3330.2	Dol2	-3.05	1.32	-
16*	C	3330.5	Dol2	−3.01	0.70	0.707082
17*	C	3331.3	Dol2	−3.10	1.51	-
18*	C	3338.3	Dol1	−2.72	1.60	-
19*	C	3339.6	Dol2	-3.21	2.06	0.707041
20*	C	3340.5	Dol2	-3.83	2.06	0.707105
21*	C	3341.1	Dol2	-4.06	2.23	-
22*	C	3342.9	Dol2	-3.75	2.22	0.707111
23*	C	3344.4	Dol2	-2.67	1.80	-
24	C	3345.6	Dol1	-1.64	1.35	-
25*	C	3346.9	Dol2	-2.08	1.31	0.707002
26	C	3348.0	Dol2	-2.98	2.67	-
27	C	3360.6	Dol1	-1.33	0.90	-
28	C	3362.8	Dol2	-2.84	2.07	-
29	C	3366.2	Dol2	-4.30	2.93	0.707170
30	C	3366.3	Dol2	-3.16	2.47	-
31	A	2833.8	Dol1	-2.67	1.38	-
32*	A	2832.9	Dol1	-2.00	0.85	0.706982
33	A	2839.4	Dol2	-2.41	0.5	-
34	A	2842.7	Dol2	-4.02	1.28	-
35*	A	2843.0	Dol2	-3.83	1.55	-
36	A	2843.4	Dol2	-2.43	1.22	-
37*	A	2850.0	Dol2	-2.45	2.04	0.707108

Note:

[1] Samples indicated with * are those used for Δ_{47}/U-Pb thermo-chronometry (see Table DR4)

[2] $\delta^{18}O_{dol}$ and $\delta^{13}C_{dol}$ are reported in per mil (‰) relative to the Vienna Pee Dee Belemnite (VPDB) st

Table DR1. Name, well of belonging, dolomite type, isotope compositions ($\delta^{18}O_{dol}$, $\delta^{13}C_{dol}$, $^{87}Sr/^{86}$

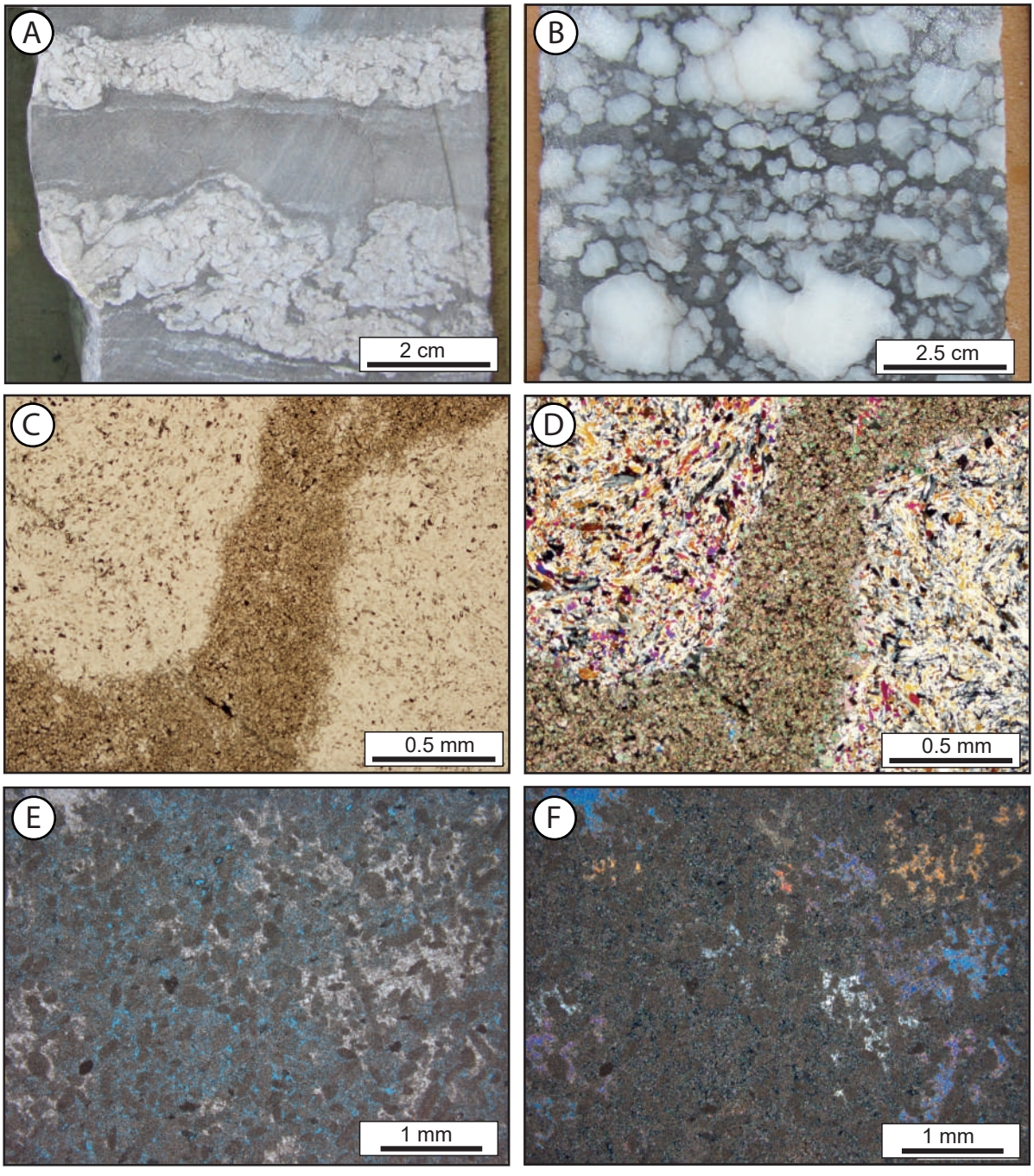
A
2 cm
B
2.5 cm
C
0.5 mm
D
0.5 mm
E
1 mm
F
1 mm

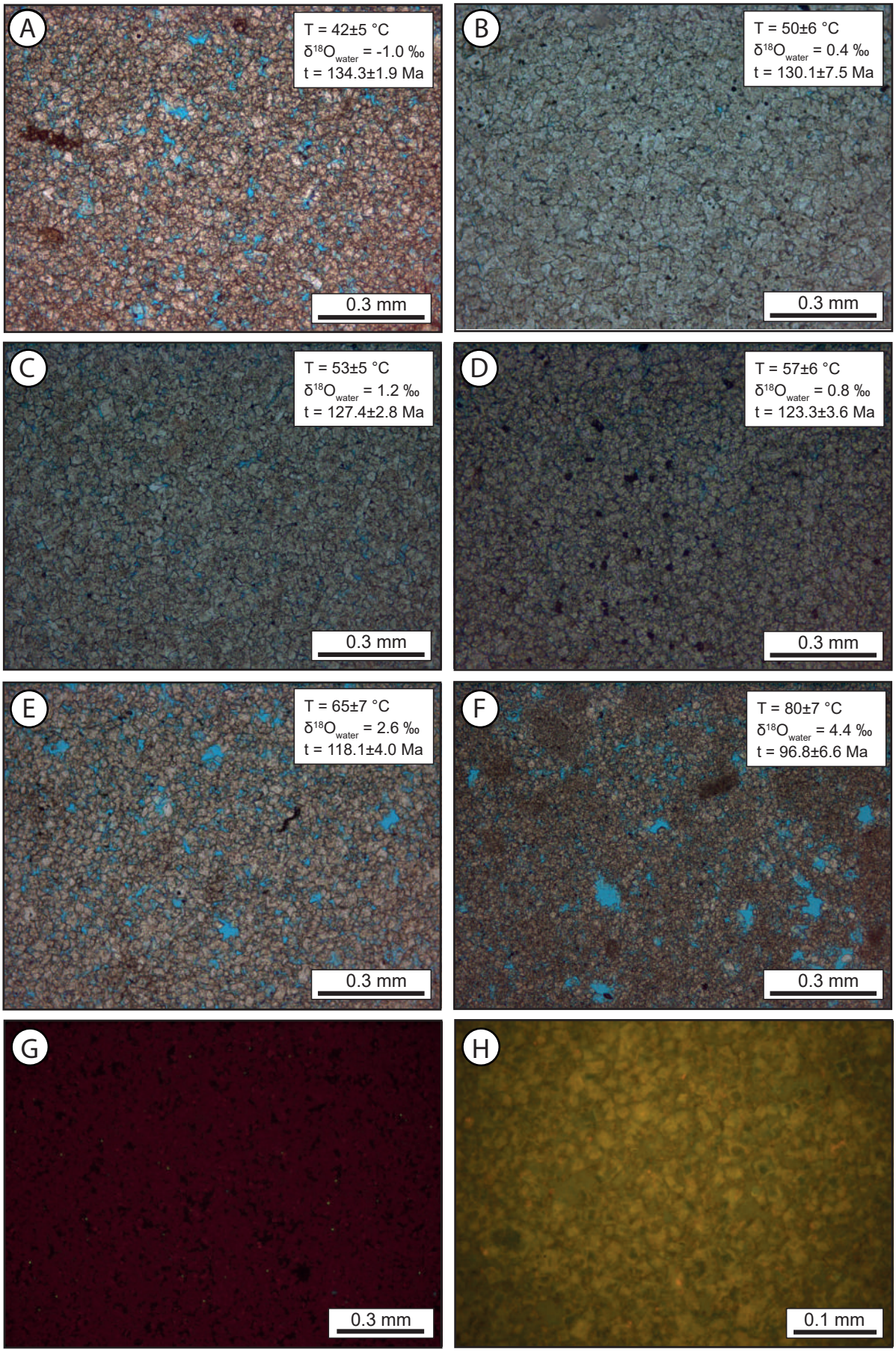
A
T = 42±5 °C
δ18Owater = -1.0 ‰
t = 134.3±1.9 Ma
0.3 mm
B
T = 50±6 °C
δ18Owater = 0.4 ‰
t = 130.1±7.5 Ma
0.3 mm
C
T = 53±5 °C
δ18Owater = 1.2 ‰
t = 127.4±2.8 Ma
0.3 mm
D
T = 57±6 °C
δ18Owater = 0.8 ‰
t = 123.3±3.6 Ma
0.3 mm
E
T = 65±7 °C
δ18Owater = 2.6 ‰
t = 118.1±4.0 Ma
0.3 mm
F
T = 80±7 °C
δ18Owater = 4.4 ‰
t = 96.8±6.6 Ma
0.3 mm
G
0.3 mm
H
0.1 mm

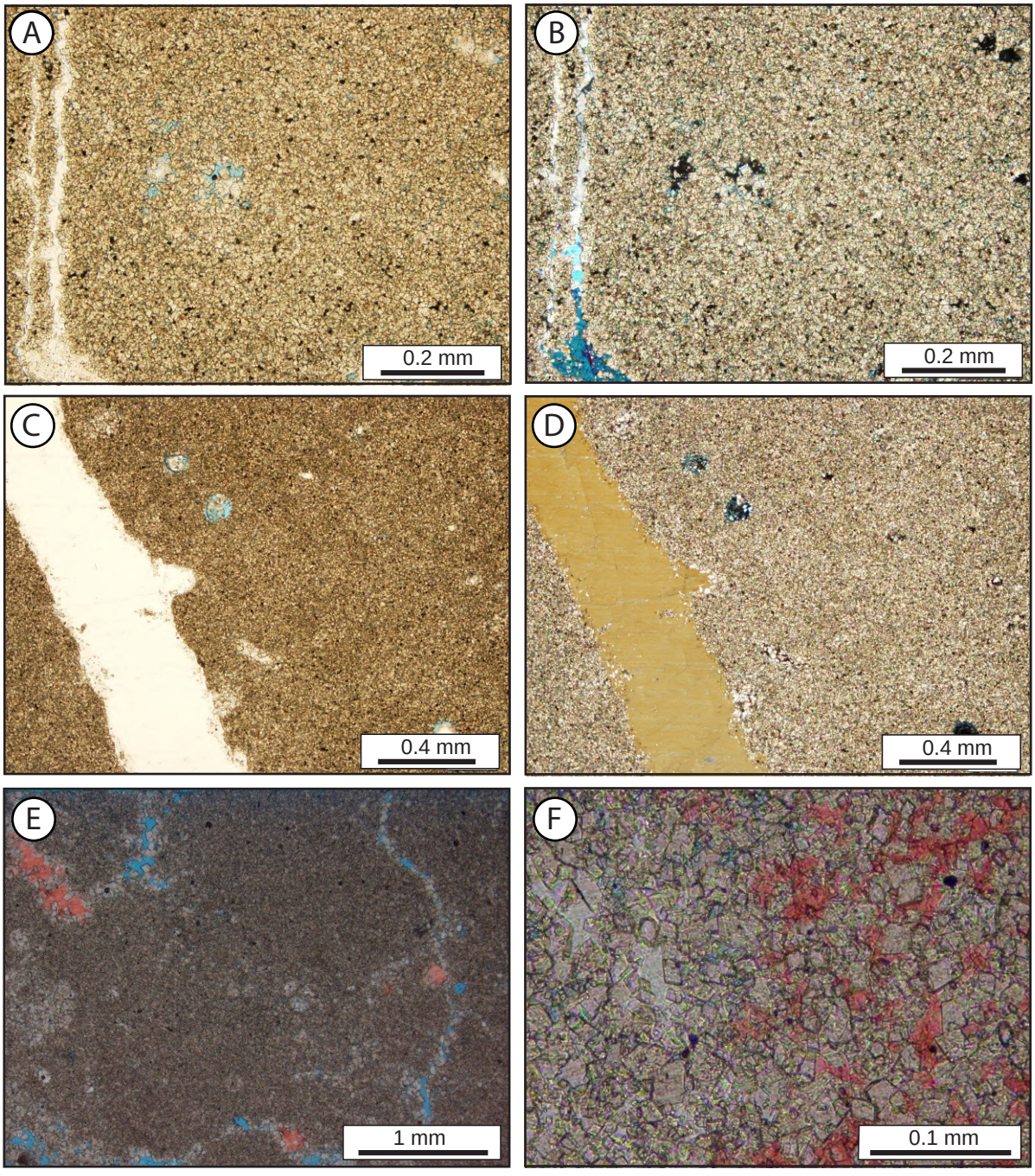
A
0.2 mm
B
0.2 mm
C
0.4 mm
D
0.4 mm
E
1 mm
F
0.1 mm

Sample ID	Well	Depth (m)	Dolomite type	CL response	UV-light response	N[1]	$\delta^{18}O_{dol}$ (‰, VPDB)[2]	$\delta^{13}C_{dol}$ (‰, VPDB)[2]	Δ_{47} (‰; CDES)[3]	$T\Delta_{47}$ (°C)[4]	$\delta^{18}O_w$ (‰, VSMOW)[5]	n[6]	U-Pb age (Ma)[7]	MSWD[8]	$^{207}Pb/^{206}Pb$[9]
4	C	3309.7	Dol2	dull red	uniform	3	−4.0±0.54	2.1±0.08	0.464±0.004	**80±7**	+4.4±1	28	**95.9±6.6**	0.72	0.813±0.006
12	C	3318.9	Dol2	dull red	uniform	3	−3.9±0.18	1.9±0.03	0.514±0.024	**57±6**	+0.8±1	72	**123.3±3.7**	1.16	0.823±0.003
15	C	3330.2	Dol2	dull red	uniform	3	−3.6±0.67	2.2±0.02	0.498±0.014	**64±6**	+2.3±1	31	**124.4±6.5**	0.51	0.821±0.005
16	C	3330.5	Dol2	dull red	uniform	3	−2.9±0.15	−0.6±0.01	0.522±0.012	**53±5**	+1.2±1	91	**128.4±2.1**	1.26	0.790±0.006
17	C	3331.3	Dol1	dull red	uniform	3	−3.2±0.50	1.4±0.02	0.529±0.016	**51±5**	+0.4±1	54	**134.4±4.4**	1.24	0.806±0.011
18	C	3338.3	Dol2	dull red	uniform	2	−3.1±0.02	1.5±0.03	0.531±0.002	**50±6**	+0.4±1	38	**130.7±6.5**	1.12	0.815±0.009
19	C	3339.6	Dol2	dull red	zoned	3	−4.5±0.12	2.2±0.03	0.452±0.07	**87±23**	+4.9±3	51	**91.6±7.6**	1.26	0.816±0.005
20	C	3340.5	Dol2	dull red	zoned	3	−3.0±0.61	1.5±0.01	0.550±0.023	**42±5**	−1.0±1	44	**136.5±1.7**	1.90	0.802±0.006
21	C	3341.1	Dol1	dull red	zoned	3	−3.8±0.33	1.4±0.16	0.545±0.019	**44±5**	−1.4±1	-	-	-	-
22	C	3342.9	Dol2	dull red	zoned	2	−3.6±0.12	1.9±0.14	0.495±0.013	**65±7**	+2.6±1	52	**118.3±4.2**	0.77	0.818±0.003
23	C	3344.4	Dol2	dull red	uniform	3	−2.9±0.68	0.1±0.08	0.511±0.014	**58±6**	+2.1±1	37	**134.8±5.5**	0.69	0.822±0.004
25	C	3346.9	Dol2	dull red	uniform	3	−2.1±0.68	1.4±0.03	0.533±0.025	**49±6**	+1.2±1	-	-	-	-
32	A	2832.9	Dol2	dull red	uniform	3	−3.8±0.06	1.6±0.01	0.498±0.003	**64±6**	+2.1±1	-	-	-	-
35	A	2843.0	Dol2	dull red	zoned	3	−4.1±0.18	1.5±0.04	0.537±0.011	**47±5**	−1.1±1	13	**135.7±4.1**	0.62	0.818±0.015
37	A	2850.0	Dol2	dull red	uniform	3	−2.0±0.48	0.9±0.01	0.536±0.006	**48±5**	+1.1±1	-	-	-	-

Note:

[1] Number of replicate measurements ($\delta^{18}O_{dol}$, $\delta^{13}C_{dol}$, Δ_{47}) of the same carbonate powder

[2] $\delta^{18}O_{dol}$ and $\delta^{13}C_{dol}$ are reported in per mil (‰) relative to the Vienna Pee Dee Belemnite (VPDB) standard

[3] Values relative to the 'carbon dioxide equilibrium scale' (CDES), n the 25°C acid digestion scheme (acid fractionation of 0.092‰). Reported uncertainties on Δ_{47} are one standard deviation of the mean (±1 SD) of replicate measurements (2<N<3) on the same powder

[4] Temperatures are computed using the composite Δ_{47} -T calibration of Bonifacie et al. (2017). Uncertainties on $T\Delta_{47}$ are calculated as SE (=SD/√N)

[5] $\delta^{18}O_w$ is reported in per mil (‰) relative to the Vienna Standard Mean Oceanic Water (VSMOW)

[6] Number of LA-ICPMS spot analyses

[7] Tera-Wasserburg U-Pb lower intercept ages. Uncertainties on the U-Pb ages are reported as 2σ

[8] MSWD - Mean Squared Weighted Deviates

[9] Isochron intercept on the y-axis is the initial $^{207}Pb/^{206}Pb$ ratio of the mineralizing fluid

Table DR4. Name, well of provenance, dolomite type, CL and UV-light response, stable isotope compositions ($\delta^{18}O_{dol}$, $\delta^{13}C_{dol}$, Δ_{47}, $\delta^{18}O_w$) and U-Pb ages of the dolomite samples investigated with Δ_{47}/U-Pb thermo-chronometry.

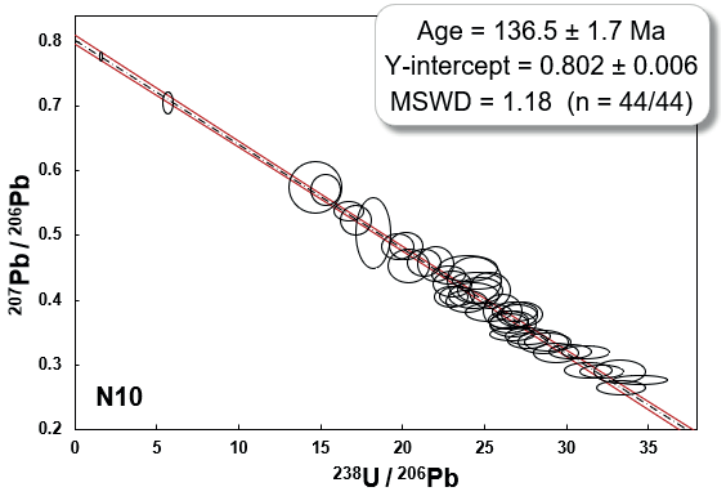
Age = 136.5 ± 1.7 Ma
Y-intercept = 0.802 ± 0.006
MSWD = 1.18 (n = 44/44)
N10
$^{207}Pb / ^{206}Pb$
$^{238}U / ^{206}Pb$

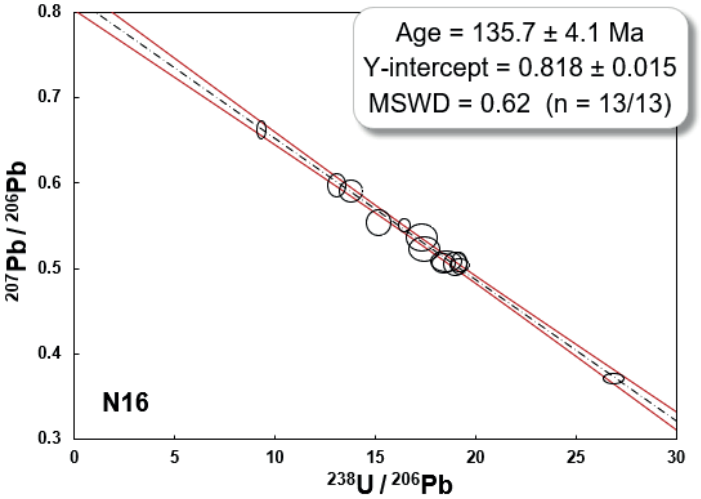
Age = 135.7 ± 4.1 Ma
Y-intercept = 0.818 ± 0.015
MSWD = 0.62 (n = 13/13)
N16
$^{207}Pb / ^{206}Pb$
$^{238}U / ^{206}Pb$

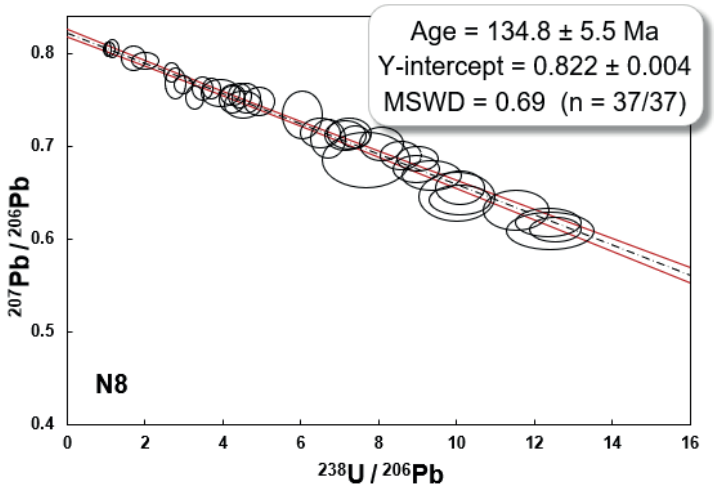
Age = 134.8 ± 5.5 Ma
Y-intercept = 0.822 ± 0.004
MSWD = 0.69 (n = 37/37)
N8
$^{207}Pb / ^{206}Pb$
$^{238}U / ^{206}Pb$

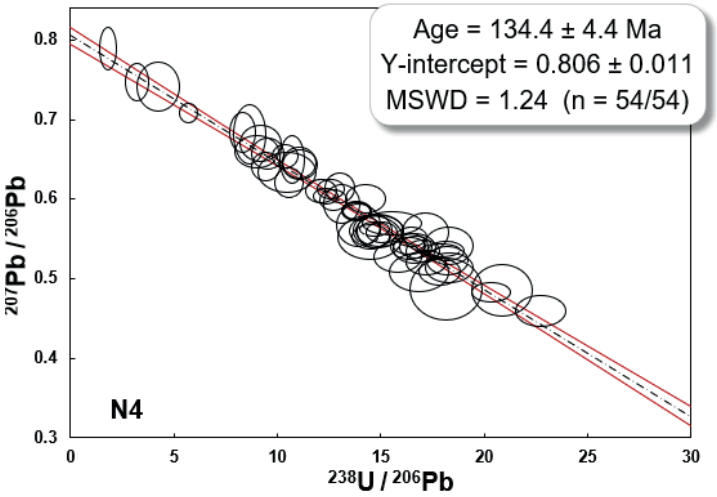
Age = 134.4 ± 4.4 Ma
Y-intercept = 0.806 ± 0.011
MSWD = 1.24 (n = 54/54)
N4
$^{207}Pb / ^{206}Pb$
$^{238}U / ^{206}Pb$

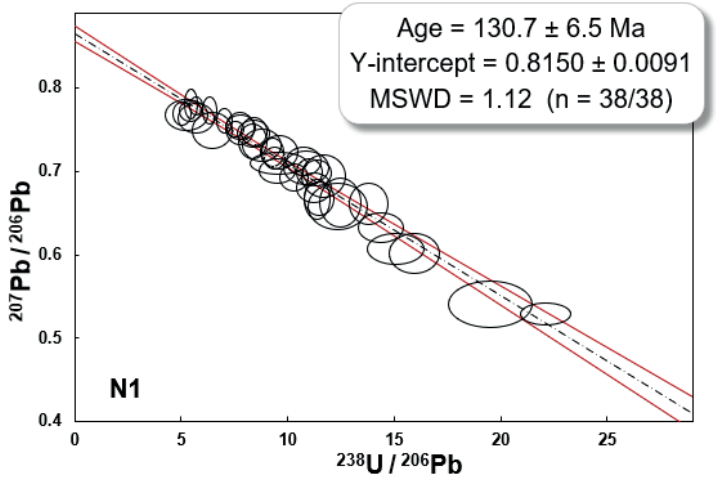
Age = 130.7 ± 6.5 Ma
Y-intercept = 0.8150 ± 0.0091
MSWD = 1.12 (n = 38/38)
N1
$^{207}Pb / ^{206}Pb$
$^{238}U / ^{206}Pb$

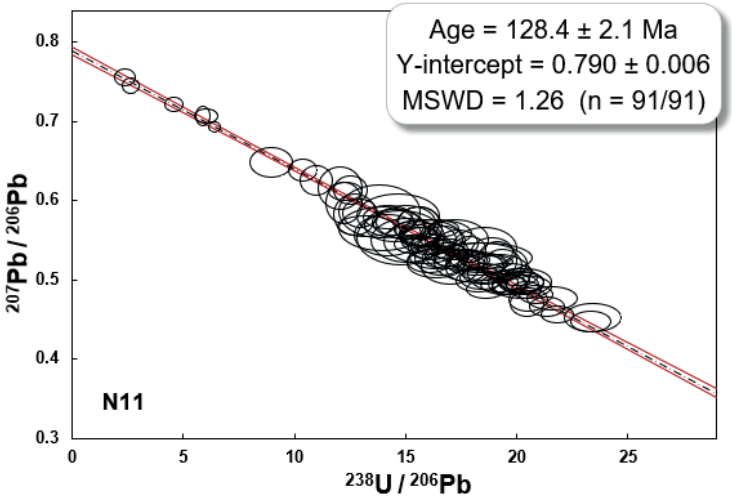
Age = 128.4 ± 2.1 Ma
Y-intercept = 0.790 ± 0.006
MSWD = 1.26 (n = 91/91)
N11
$^{207}Pb / ^{206}Pb$
$^{238}U / ^{206}Pb$

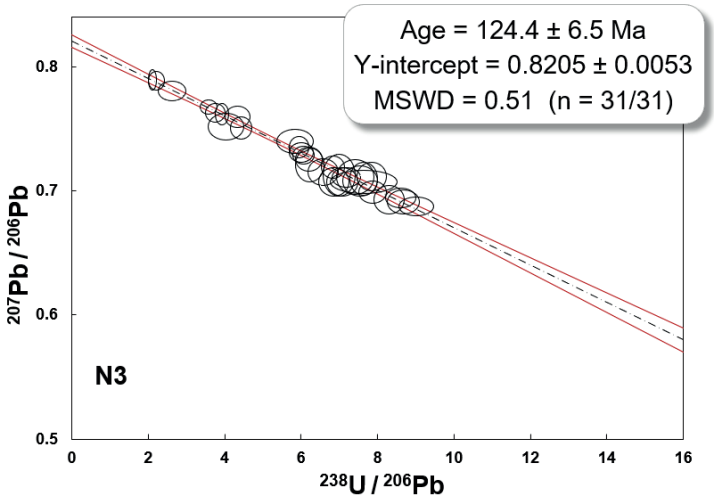
Age = 124.4 ± 6.5 Ma
Y-intercept = 0.8205 ± 0.0053
MSWD = 0.51 (n = 31/31)
N3
$^{207}Pb / ^{206}Pb$
$^{238}U / ^{206}Pb$

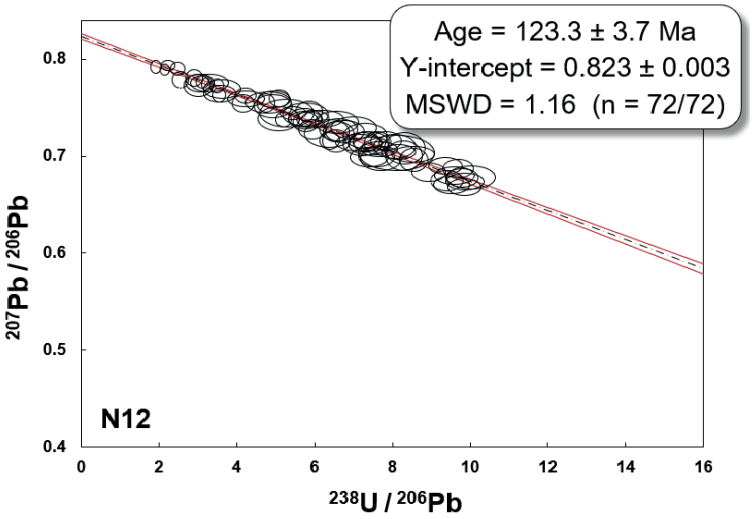
Age = 123.3 ± 3.7 Ma
Y-intercept = 0.823 ± 0.003
MSWD = 1.16 (n = 72/72)
N12
$^{207}Pb / ^{206}Pb$
$^{238}U / ^{206}Pb$

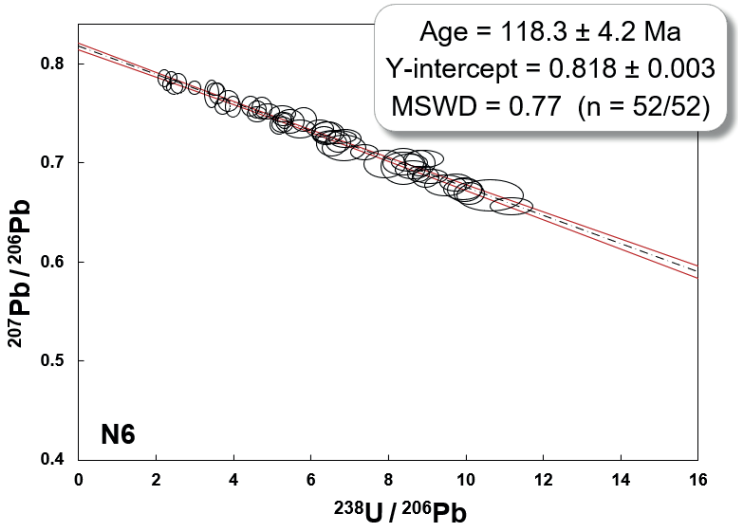
Age = 118.3 ± 4.2 Ma
Y-intercept = 0.818 ± 0.003
MSWD = 0.77 (n = 52/52)
N6
$^{207}Pb / ^{206}Pb$
$^{238}U / ^{206}Pb$

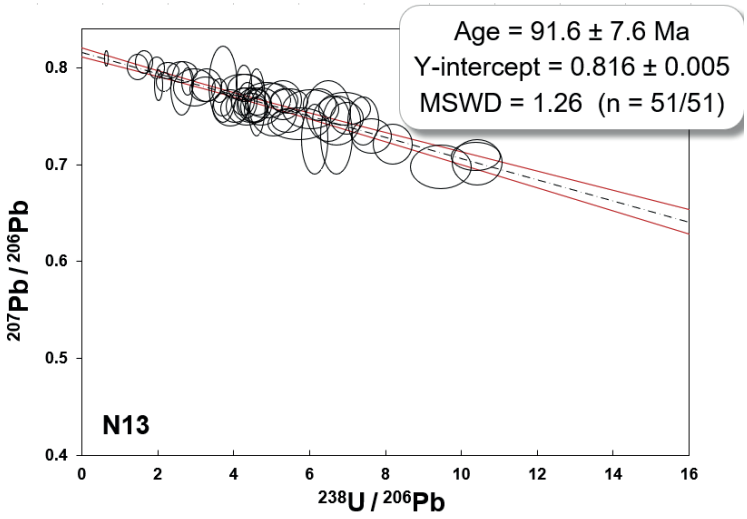
Age = 91.6 ± 7.6 Ma
Y-intercept = 0.816 ± 0.005
MSWD = 1.26 (n = 51/51)
N13
$^{207}Pb / ^{206}Pb$
$^{238}U / ^{206}Pb$

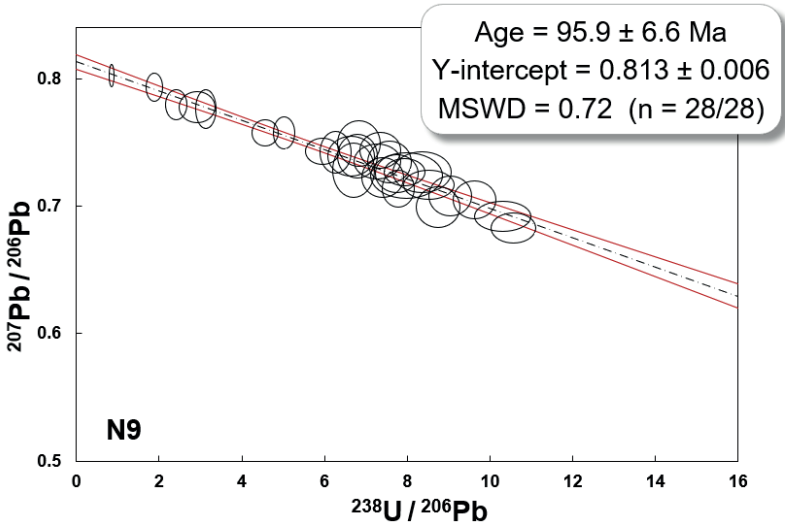
Age = 95.9 ± 6.6 Ma
Y-intercept = 0.813 ± 0.006
MSWD = 0.72 (n = 28/28)
N9
$^{207}Pb / ^{206}Pb$
$^{238}U / ^{206}Pb$

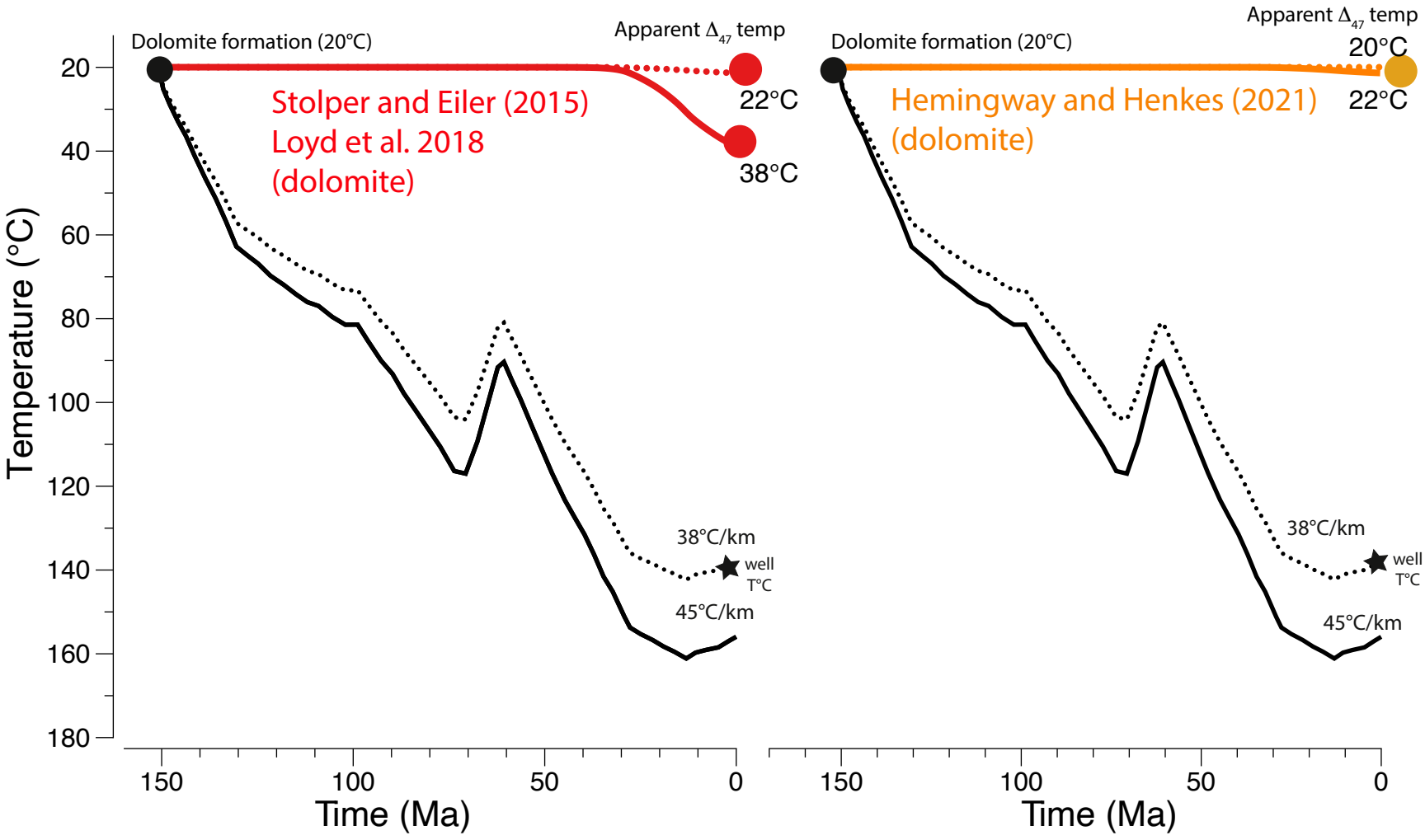
Dolomite formation (20°C)
Apparent Δ47 temp
Stolper and Eiler (2015)
Loyd et al. 2018
(dolomite)
22°C
38°C
38°C/km
well
T°C
45°C/km
Temperature (°C)
20
40
60
80
100
120
140
160
180
150
100
50
0
Time (Ma)
Dolomite formation (20°C)
Apparent Δ47 temp
Hemingway and Henkes (2021)
(dolomite)
20°C
22°C
38°C/km
well
T°C
45°C/km
150
100
50
0
Time (Ma)